

# Reinventing the Automobile: Designing a Lighter Class of Road Vehicle

A Study Conducted for the Center for Environmental Studies, Harvey Mudd College

Steven Ning  
Harvey Mudd College

October 5, 2009

# Contents

<b>1 Introduction</b>	<b>3</b>
1.1 Motivation . . . . .	3
1.2 A Concept Light Vehicle Design . . . . .	3
<b>2 The Project</b>	<b>4</b>
2.1 Objective and Goals . . . . .	4
2.2 Project Outline . . . . .	4
<b>3 Methodology and Discussion</b>	<b>5</b>
3.1 Modeling Deformation of a Steel S-Beam . . . . .	5
3.2 Modeling Spot Welds and Part Attachments . . . . .	7
3.3 A Simple Bumper Collision Test . . . . .	9
3.4 Importing LS-DYNA Vehicle Collision Models Into ABAQUS Using KEY2INP.PY . . . . .	11
3.5 Material Failure Modeling . . . . .	13
3.6 Modeling Wheel Rims . . . . .	14
3.7 Creating a Spoked Wheel with MAKESPOKES.PY . . . . .	16
3.8 Collision Testing of Spoked Wheel Designs . . . . .	18
3.9 A Simple Crash Dummy Model . . . . .	22
3.10 Creating the Light Vehicle Prototype . . . . .	23
<b>4 Recommendations for Future Work</b>	<b>25</b>
<b>5 Environmental Applicability and Concluding Remarks</b>	<b>26</b>
<b>6 Acknowledgments</b>	<b>27</b>
<b>7 Appendix: Accessing the Online Research Journal</b>	<b>28</b>
<b>References</b>	<b>29</b>

# 1 Introduction

## 1.1 Motivation

Gasoline-powered automobiles will one day be replaced by lighter and more efficient vehicles which emit less carbon dioxide. Electric vehicles have arrived on the market as a first step towards achieving this goal, but they are by no means light. The original GM EV1 weighs around 3000 lbs[10], the Chevy Volt has a quoted curb weight of over 3500 lbs[4], the Dodge Circuit EV 2980 lbs[5], and the Nissan Leaf is estimated at 2800 lbs[10]. In comparison, a large gasoline-powered passenger sedan has a curb weight in the neighborhood of 3600 lbs. Thus, modern electric sedans can be classified with gasoline-powered sedans as “heavy” vehicles.

On the other end of the spectrum, motorcycles and scooters, weighing under 500 lbs, are by far the most efficient vehicles on the road today. However, this efficiency comes at a great cost. Conservation of momentum in vehicular collision dictates in general that the lighter vehicle’s occupants are subject to greater decelerations, thus they have a higher probability for injury. Motorcycles also offer minimal occupant protection - indeed, survival in a head-on collision with an automobile hinges on how well the rider escapes the motorcycle upon impact.

We seek some form of intermediate road vehicle which is light enough to offer substantially improved efficiency over heavy vehicles, yet also provide a significant means of occupant protection in the event of vehicular collision. Such a vehicle will likely be substantially heavier than a motorcycle, and lies in a class of its own, which for purposes of this study we will term the “light vehicle” class.

The preponderance of heavy vehicles on the road today suggests that progress towards generally lighter road vehicles will be an evolutionary one at best - unless revolutionary occupant protection mechanisms can be developed for these lighter vehicles. This work is intended as a plausibility study of a novel occupant protection mechanism for a conceptual two-wheel, single occupant light vehicle, intended to fill the gap between heavy vehicles and motorcycles.

## 1.2 A Concept Light Vehicle Design

A two-wheeled vehicle design has been developed to serve as the basis for the current study. This design places the rider in a reclined fashion between two large ( $> 1$  m diameter) spoked wheels, in a layout similar to that of a recumbent bicycle. A two wheeled design has a number of advantages over a four-wheeled design - two large wheels offer in general lower coefficients of rolling friction than four small wheels, and the in-line layout of the two wheels allows for a narrow frontal profile, which helps reduce aerodynamic drag.

The front wheel in this design is intended to provide a measure of impact absorption during collision with a heavy vehicle, and to allow for deflection of the rider over the collision zone. Such a wheel may be designed to simply deflect the trajectory of the entire vehicle over the hood of the impacting vehicle, or the rider’s

seat may be designed to lift or swing the occupant out of the collision area upon impact. In either case, care must be taken so that the resulting motion of the light vehicle does not cause it to enter the impacting heavy vehicle's windshield.

## **2 The Project**

### **2.1 Objective and Goals**

The objective for this project is to model and characterize an occupant protection mechanism for the light vehicle design discussed above. For this project, we use the finite-element simulation software ABAQUS to simulate the behavior of vehicle components in deformation scenarios such as collision. Goals set out for this project include

- Development of proficiency using the ABAQUS software for modeling, material definition, and collision simulation
- Subdivision of the light vehicle design into separate, independently modeled and tested components
- Validation of physical accuracy of component simulations via comparison to published experimental or simulation results
- Demonstration of successful integration of these components into a final prototype model
- Simulation of the prototype in collision with a standard passenger sedan model or analogue
- Development of a system to measure forces transmitted to the occupant during collision in a way which would allow direct comparison to National Highway Safety Administration (NHTSA) occupant protection standards[1, 2]

### **2.2 Project Outline**

This project was framed as a six-week study, and the following milestones were set during the first two weeks of the study to serve as a tentative guideline and schedule:

Week	Tasks
1	Order Research Edition of ABAQUS
	Conduct general literature search on finite-element modeling
	Obtain evaluation version of ABAQUS and begin creating practice simulations
2	Conduct literature search on crash testing and simulation
	Reproduce results of a simple finite-element simulation in ABAQUS
	Begin modeling structural members for use in simple collision simulations
3	Model and test wheels for use in light vehicle prototype model
	Investigate methods for creating representation of passenger sedan as a “crash target”
4	Model and test chassis design for light vehicle
	Model a passenger sedan analogue to serve as a crash target
5	* Simulate chassis design in collision with car analogue
	* Obtain and tabulate force and deceleration measurements
6	* Complete simulations, compare results with NHTSA guidelines
	Compile results into final report

The actual timeline taken in the course of this project, however, deviated from this guideline. Milestones past Week 3 were achieved in a delayed fashion, and milestones denoted with (\*) were not completed within the six-week time period. Significant progress, however, was made in overcoming challenges towards the final milestones, as will be discussed in the following sections.

### 3 Methodology and Discussion

#### 3.1 Modeling Deformation of a Steel S-Beam

As an introductory exercise in modeling material deformation in ABAQUS, we attempt to reproduce the results of a study by Kim and Huh[9]. In their paper, Kim and Huh simulate the behavior of a hollow steel s-beam placed under axial compression in ABAQUS. The beam is characterized as a 50 cm × 6 cm × 6 cm square tube in an S-shape, with a thickness of 0.7 mm. It is compressed 20 cm, and reaction force from the beam is measured as a function of compression distance. A simple mathematical expression is used to describe work-hardening in the material for the beam, and serves as the material definition.

It is unclear whether Kim and Huh model their s-beam using 2D or 3D mesh elements. For this exercise we use 2D shell elements, in which the thickness of the element is represented computationally as an additional stiffness for deformations normal to the shell element. In situations where the thickness of the element

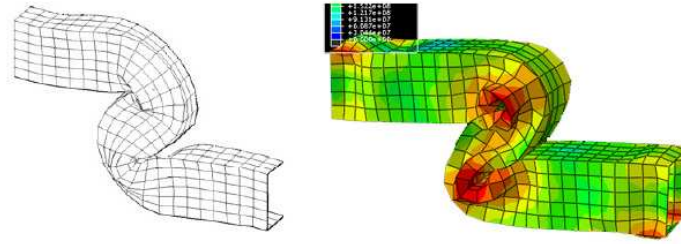
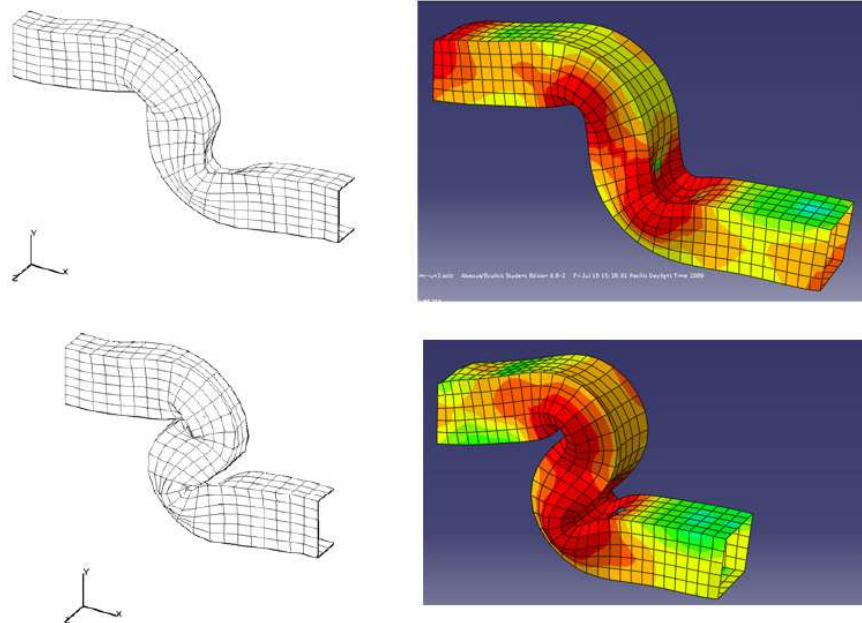


Figure 1: Kim and Huh Result, First Simulation Result - A Comparison



(a) Kim and Huh Results (half-shells only)

(b) Second Simulation Results

Figure 2: S-Beam Compression Comparison

is small relative to the lateral dimensions, shell elements offer much faster simulation times with minimal impact on accuracy.

The results of the first simulation run are shown in Figure 1 . It is obvious that there is something wrong with the material or mesh definition - the beam does not deform in the manner suggested by Kim and Huh.

Reasoning that perhaps the authors had made a mistake quoting the thickness of their s-beam, we try instead using a thickness of 7 mm. The results show better qualitative agreement with Kim and Huh’s results, as shown in Figure 2 .

The method by which the authors measure reaction force in the s-beam is not specified in their paper. For this exercise, we choose to measure values for axial stress on the vertices at the moving end of the s-beam, and then average over those values to obtain a plot of reaction force with respect to compression distance. A comparison with the results of Kim and Huh is given in Figure 3 .

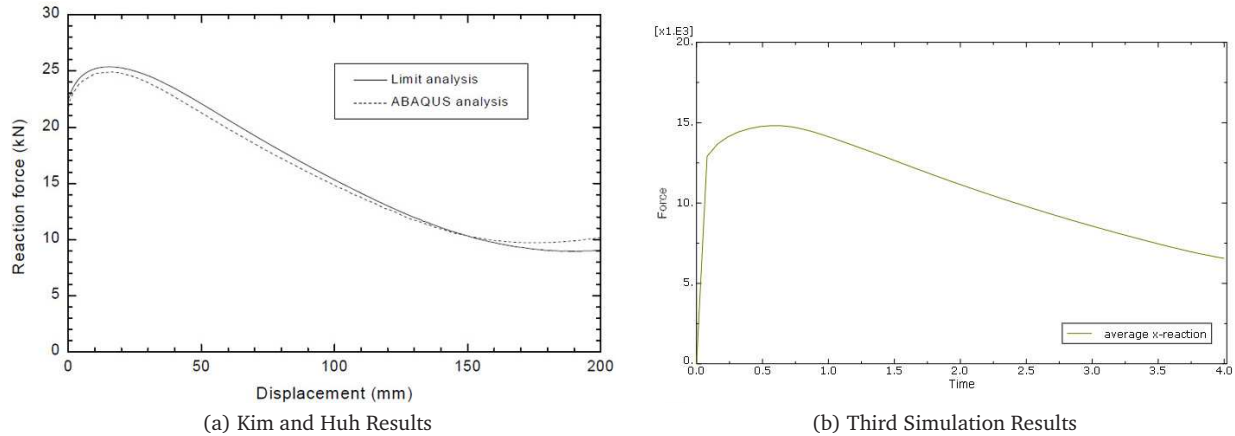


Figure 3: S-Beam Reaction Force Comparison

There are some important differences to note. First, the maximum force magnitudes during compression do not agree. Although it was not immediately clear what the reason for this may be, we have realized in subsequent experience with 2D shell elements that the simulation engine decreases the computational thickness of a shell element if it cannot accurately simulate deformation of the element. At the time, however, I was unfamiliar with this caveat and the discrepancy was left as an open question.

The shapes of the reaction force curves agree to some extent, but there is an interesting curve upwards towards the end of the compression cycle in Kim and Huh’s model which is not evident in our model. This may be due to the fact that the s-beam modeled in the paper has a finer mesh than the one created for this exercise. A finer mesh, however, was not possible at the time this model was created. The Student Edition of ABAQUS, which limits the number of mesh elements on the model, was used for this exercise while waiting for the Research Edition of ABAQUS to arrive.

While this exercise did not produce results in exact agreement with the referenced study, it served as a fast and effective crash-course in material deformation modeling, taking only two days to complete.

### 3.2 Modeling Spot Welds and Part Attachments

Realizing that a more complex collision model would require attachments to be defined among constituent parts, we conduct an exercise to model spot-welds between deforming parts. It became clear during a literature search prior to this project that structural members in automobiles are fastened together almost exclusively using spot-welds. Furthermore, spot-welds rarely fail in vehicular collisions - the weak points lie instead in the deformation zones of buckling structural members[3]. Thus, the goal of this exercise was to model indestructible point-based attachments between two parts. ABAQUS offers a simple method for creating such attachments - point-based fasteners are defined at a single point on which the “weld” is to be centered. Prior to simulation, vertices within a specified radius of the weld are fastened together with a rigid-body constraint.

The setup created for this exercise is shown in Figure 4 . A hollow tube of extruded steel is welded at eight

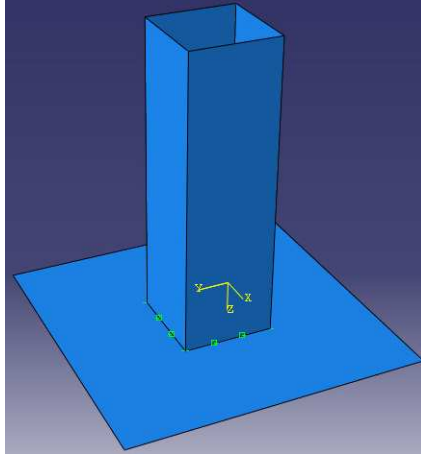


Figure 4: Weld Shear Test Setup

Parameter	Value	Parameter	Value
Density	$7850 \frac{\text{kg}}{\text{m}^3}$	Density	$7850 \frac{\text{kg}}{\text{m}^3}$
Modulus of Elasticity	207 GPa	Modulus of Elasticity	207 GPa
Poisson's Ratio	0.3	Poisson's Ratio	0.3
Johnson-Cook $\dot{\epsilon}_0$	$1 \frac{1}{\text{s}}$	Johnson-Cook $\dot{\epsilon}_0$	$1 \frac{1}{\text{s}}$
Johnson-Cook $A$	217 MPa	Johnson-Cook $A$	430 MPa
Johnson-Cook $B$	233.7 MPa	Johnson-Cook $B$	823.6 MPa
Johnson-Cook $n$	0.6428	Johnson-Cook $n$	0.5071
Johnson-Cook $C$	0.0756	Johnson-Cook $C$	0.0171

(a) Mild Steel

(b) DP590 Steel

Table 1: Material Parameters for Steel Definitions

points (denoted by yellow squares) to a steel plate. The edges of the steel plate are held fixed while the top edge of the steel tube is given rotational displacement. Results at a number of time steps are presented in Figure 5 .

This exercise also made use of a more complex material definition for steel. The Johnson-Cook plasticity model is an empirical model which describes isotropic work-hardening in a deforming material. The general expression for yield stress in the Johnson-Cook formulation (discounting temperature dependence) is

$$\sigma = [A + B\epsilon^n] \left[ 1 + C \ln \left( \frac{\dot{\epsilon}}{\dot{\epsilon}_0} \right) \right]$$

where  $\epsilon$  is the plastic strain;  $\dot{\epsilon}$  is the strain rate;  $A$ ,  $B$ ,  $C$ , and  $n$  are material specific parameters; and  $\dot{\epsilon}_0$  is the reference strain rate for which the parameters are measured. The material-specific parameters for a Johnson-Cook formulation of Dual Phase (DP) 590 steel are taken from a study by Vedantam et al, and used to create the material definition for steel used in this exercise[11]. All material parameters used in this definition appear in Table 1b . Dual Phase steels are commonly used in automobile structural members, and



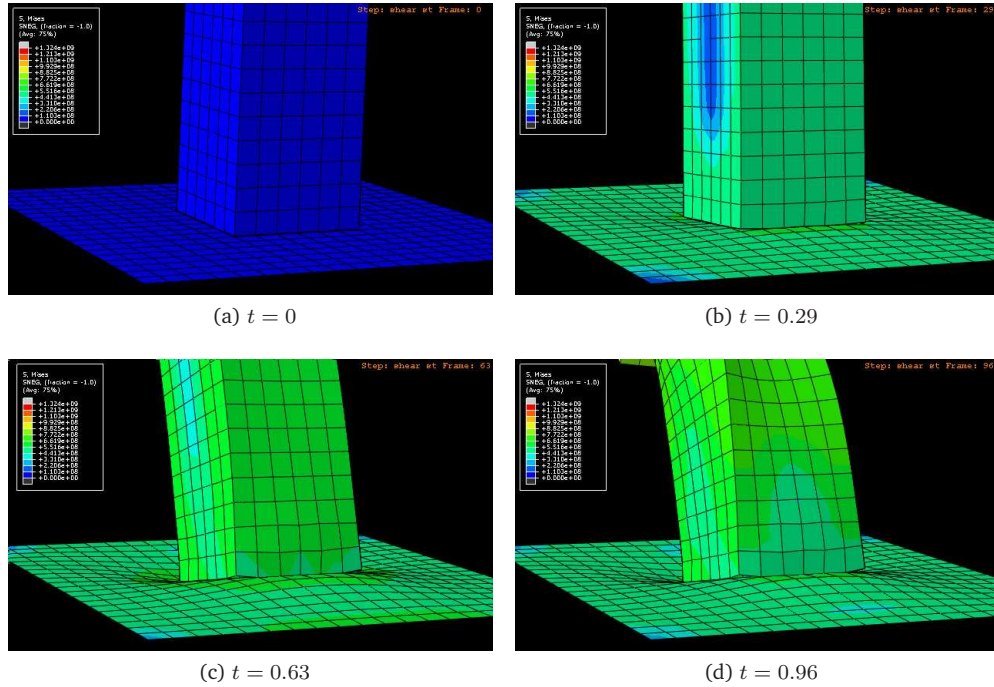


Figure 5: Weld Shear Simulation

it seemed appropriate to keep this material definition for use in subsequent models for this project.

### 3.3 A Simple Bumper Collision Test

Experience gained from the previous two exercises allowed for the creation of an elementary collision model. Two s-beams are welded to a straight beam, forming a simple bumper, and a point mass is attached to the bumper via the rear edges of the s-beams. This system is accelerated and allowed to collide with a rigid stationary wall. The setup is illustrated in Figure 6 . Spot-welds on the s-beams are denoted by yellow squares and dynamic constraints by yellow circles.

The material definition used in this model is based on the properties of mild steel, with Johnson Cook parameters taken from Vedantam et al[11]. A summary of the parameters used in this material definition appears in Table 1a. Parameters for each part in the assembly are summarized in Table 2 . The point mass used in the model incorporates a large (non realistic) moment of rotational inertia for each axis of rotation to prevent the bumper assembly from pivoting. This is used primarily as a system constraint rather than as representation of a physical property of the bumper-mass system.

Definitions for contact properties between surfaces are used extensively during this exercise. Contact constraints are enforced when the simulation engine detects overlap or penetration (overclosure) between two surfaces, or between a node and a surface. ABAQUS provides a number of different ways to handle overclosure. In the direction normal to the surfaces, one can choose “hard” and “soft” constraint enforcement. Hard enforcement minimizes overclosure, and soft enforcement allows for variation of normal force with

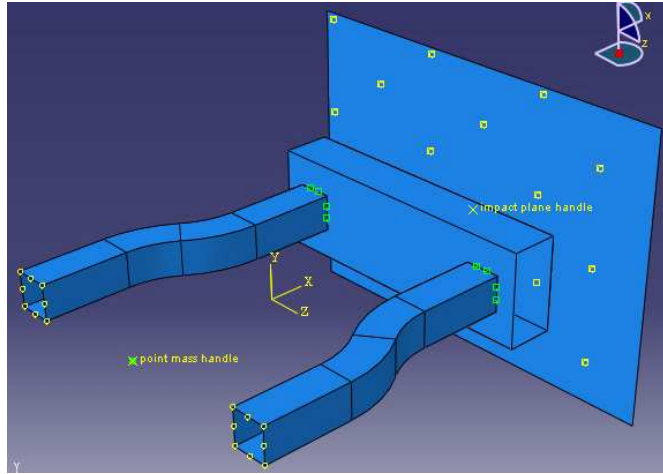


Figure 6: Bumper Test Setup

Part	Property	Value
S-Beam	Dimensions	6 cm × 6 cm × 50 cm
	Thickness	10 mm
	Material	Mild Steel
	Mass	9.67 kg each
Straight Beam	Dimensions	8 cm × 16 cm × 50 cm
	Thickness	10 mm
	Material	Mild Steel
	Mass	18.84 kg
Point Mass	Inertia	600 kg
	Rotational Inertia	1,000,000 kg · m <sup>2</sup>

Table 2: Bumper Test, Part Parameters

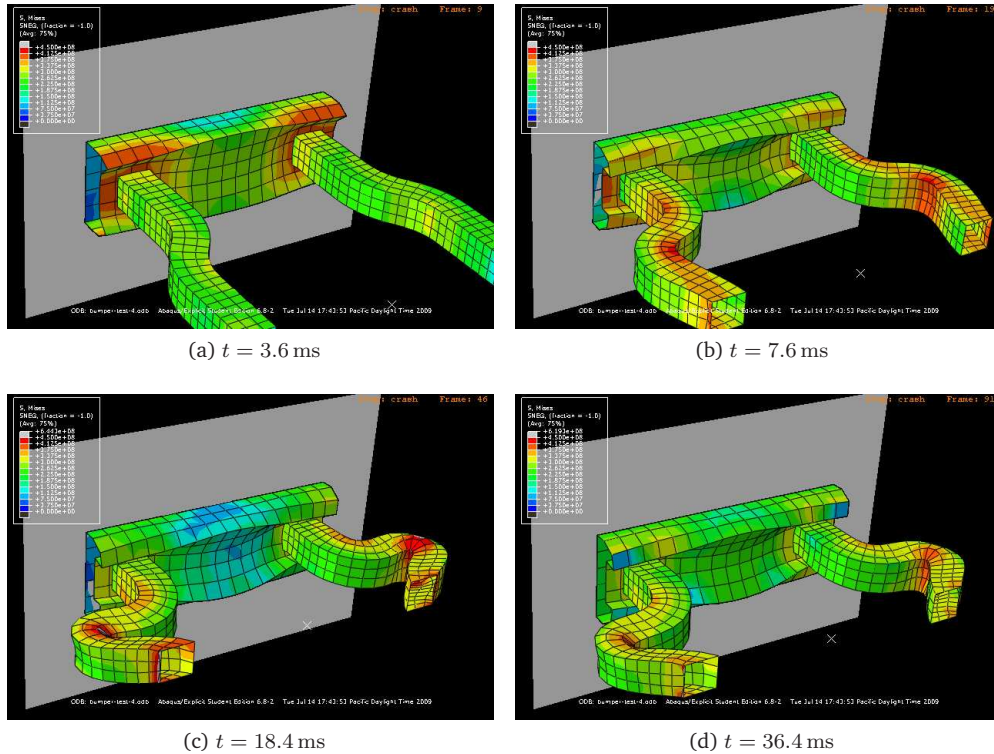


Figure 7: Bumper Collision Simulation

overclosure distance (usually positively exponential). In the direction tangential to the surfaces, one can specify frictionless contact or no-slip contact, or explicitly define coefficient of friction as a function of slip rate. For this exercise, we use a simple contact definition incorporating hard overclosure enforcement and no-slip contact, applied to all surfaces in the model.

The entire bumper assembly is given an initial velocity of  $10 \frac{m}{s}$  via instantaneous acceleration during a sub-millisecond time-interval at the beginning of the simulation. This method of setting initial velocities in ABAQUS does not create transient stresses in the material, nor does it create numerical instabilities. It is used as the preferred method for defining initial velocities in all subsequent simulations in this project.

The collision simulation covers a 40 ms time window. Results at a number of time steps are presented in Figure 7 . Color on the mesh represents Von Mises stress, and the stress scale is given on the legend in the upper left corner. A plot of acceleration with respect to time is given in Figure 8 .

### 3.4 Importing LS-DYNA Vehicle Collision Models Into ABAQUS Using KEY2INP.PY

The National Crash Analysis Center (NCAC) maintains a number of validated vehicle meshes for collision simulation in LS-DYNA, the de-facto industry standard vehicle collision modeling software. It was decided at this juncture in the project that it may be beneficial to use one of the NCAC vehicle models as a crash target for the prototype light vehicle design. At first glance, this did not seem to be a significant challenge - the “.key”

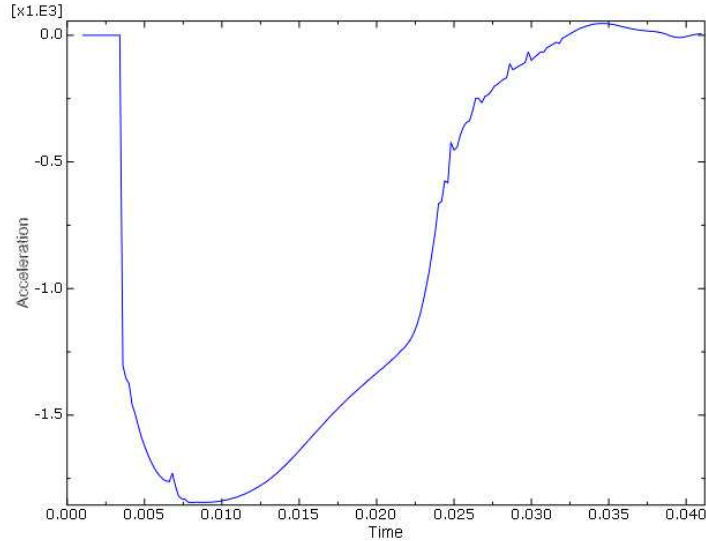


Figure 8: Bumper Point-Mass Acceleration vs. Time

model definition files used for LS-DYNA share many characteristics with the “.inp” model definition files for ABAQUS. Each file format contains a list of nodes (vertices) in the model, a list of mesh elements referencing the nodes, a number of section definitions describing behavior and material of each mesh element, a number of material definitions, and part definitions which tie these together for each part in the model.

The mesh element types provided by LS-DYNA are in large part analogous to those provided by ABAQUS - there are 1D beam and truss elements, 2D shell elements, and 3D solid elements. Vehicle models in the NCAC database consist mostly of 2D quadrilateral elements using the “Belytschko-Tsay” (BT) element formulation. This formulation requires force and energy to be integrated only at a single point at the center of the element during a computational cycle. However, Belytschko-Tsay mesh elements can also exhibit vibrational modes known as “hourglass modes,” named for the hourglass shape formed by neighboring elements during vibration. The energy in these hourglass modes do not appear at the integration point, however, so energy balance and dissipation rules cannot be used to control the vibrations. Left unchecked, these vibrations give rise to numerical instabilities whereby the hourglass modes propagate from element to element while growing in magnitude[7]. LS-DYNA provides a number of mechanisms by which hourglass mode vibrations in BT elements may be artificially damped.

There is a similar but not identical 2D quadrilateral element available in ABAQUS. Referred to as “S4R”, it also uses a reduced integration formulation comparable to Belytschko-Tsay, and includes an option for “Hourglass Control” to damp hourglass mode vibrations. Reasoning that this may allow for a close-enough translation of an LS-DYNA vehicle model to ABAQUS for the purposes of this project, we began development of a PYTHON script KEY2INP.PY to perform the translation between LS-DYNA .key format to ABAQUS .inp format.

The LS-DYNA .key file definition incorporates a large number of unforeseen inconsistencies and idiosyncrasies, which made the process of writing a translation script mostly an exercise in perseverance. In the end, however, after a functional version of the script was tested, a new and more troubling issue was uncovered. The order in which element definitions specify their constituent nodes does not seem to be consistent

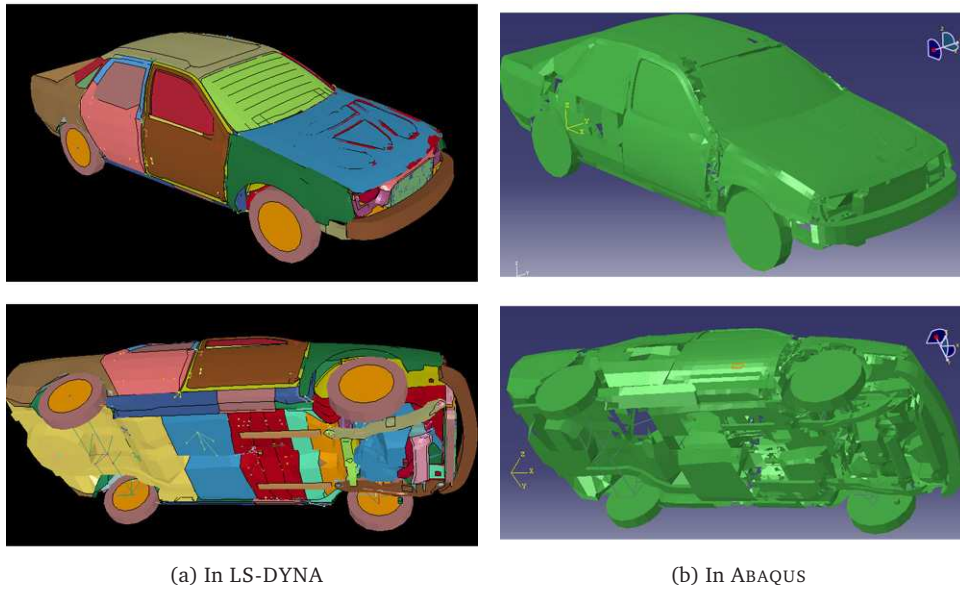


Figure 9: KEY2INP.PY Example Output

in LS-DYNA .key files - these are usually specified going around the edge of the element, but are occasionally specified in a cross-wise order. This issue manifests in the generated ABAQUS .inp file as corrupted elements, and show up as holes in the mesh, as demonstrated in Figure 9 .

After already having spent a week on the translation script, it was not prudent to invest any more time in this endeavor, and development of KEY2INP.PY was discontinued. Perhaps the most useful outcome of this incomplete effort was a much more detailed understanding of finite-element model definition and of reduced-integration mesh element behavior. This experience would come in handy - subsequent models for this project would often utilize the “S4R” element type.

### 3.5 Material Failure Modeling

A given material will fracture and fail when placed under a stress specified by the tensile strength of the material. For metals, this failure is usually preceded by necking and weakening of a localized region[8]. We require a method for describing such failures in metal structural members in order to produce meaningful collision simulation results. ABAQUS provides a convenient framework for failure modeling whereby mesh elements may be removed from simulation after reaching a specified deformation threshold. In steel, this threshold is usually in the neighborhood of 25-30%, measured by tensile testing.

By this stage of the project, we had decided upon testing a wheel design utilizing spokes. Accurately describing failure of these spokes during collision was a key goal. We conduct tensile test simulations on three different representations of a single spoke - one utilizing 1D beam elements, one utilizing 1D truss elements, and one utilizing 3D solid elements. The 1D models each consist of a spoke divided into ten linear mesh elements of equal length. The 3D model consists of a cylinder subdivided into ten axial segments, each of which is further subdivided into an equal number of triangular prisms. DP590 steel is used as the material

for these spoke representations, and the deformation threshold is set to 25%. The previously cited study by Vedantam et al serves as the experimental reference for this exercise.

For the first tensile test, each spoke is held fixed at one end while the other end is “pulled” with a linear displacement in time. The results for this test are uniformly promising. The rate dependence of strain hardening for DP590 is very low, and thus it is permissible to compare results from the simulation with those from tensile tests conducted by Vedantam et al at a strain rate of  $1 \frac{1}{s}$ . The stress-strain curves generated from the simulations indicate yield strengths which are within 5% of the measured yield strength of DP590.

There are, however, notable differences in stress-strain behavior between spokes utilizing 1D mesh elements when compared to spokes utilizing 3D mesh elements. The 3D spoke exhibits clear necking behavior on the generated stress-strain plot, while the 1D spokes show a much more linear approach toward yield stress. In ABAQUS, element failure is a continuous process in which the mesh element progressively loses strain energy (or alternatively, restoring force) as the strain proceeds beyond the failure threshold. When the additional strain exceeds a specified level, the strain energy for the element is set to zero and the element is removed from stress-strain interactions with the rest of the mesh. This additional strain allowance was set to 1% in this exercise to allow for quick failure. In general, a 1D spoke is preferable to a 3D spoke in terms of computing efficiency, and although it seems possible to mimic necking in a 1D spoke using an appropriate progressive failure definition, we reason that for rapid spoke failure in collision, necking behavior would be insignificant, and that a 1D spoke would probably suffice used as-is.

For the second tensile test, the spokes are held vertically with the bottom end affixed to a mass. The system is allowed to fall for a given time, after which the top of the spoke is suddenly stopped. The mass is allowed to vertically oscillate. This test was designed to investigate the behavior of the different spoke types under dynamic loading and unloading. It quickly became clear that the 1D beam representation of the spoke is ill-suited to model this kind of behavior - the transient vibrations generated in the spoke create numerical instabilities, crashing the simulation with an error stating that “deformation rate exceeds the speed of sound”. The truss and solid spokes, however, behaved well under sudden loading and exhibited the expected oscillation after the fall is stopped. In the end, the 1D truss element based spoke was chosen for use in a spoked wheel model.

### 3.6 Modeling Wheel Rims

Rims used for bicycle wheels are typically made of extruded aluminum tube of uniform thickness[6]. We reasoned, however, that a stronger rim would be required for use in a road vehicle designed to withstand collisions with automobiles. This phase of the project was intended to test three different rim designs for stress distribution following deformation of the rim. These tests were conducted on 2 m diameter rims of DP590 steel.

The first rim has a cross-section with a U-shape characteristic of bicycle wheel rims. It is created with S4R shell elements uniformly 3 mm thick, and the calculated mass of the rim is 55 kg. The rim is placed vertically on top of a rigid surface, and a second rigid surface moves downward to compress the rim to a final height of 50 cm in 100 ms. Figure 10 shows a side view of the rim during compression (the rigid surfaces are not



Figure 10: Rim1 Under Compression

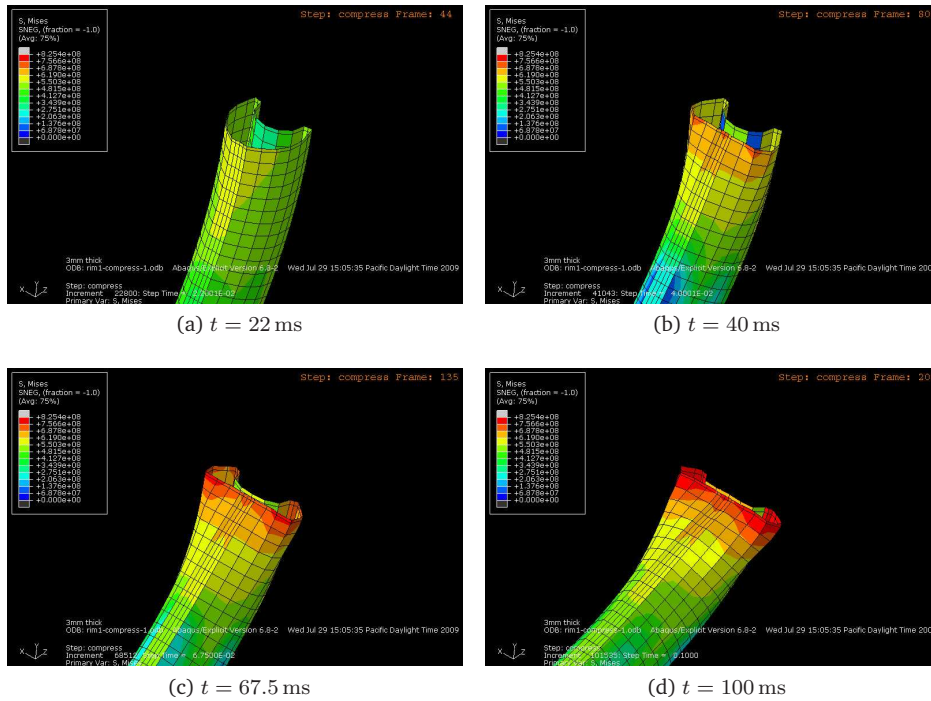


Figure 11: Rim1 Compression, Cutaway Views

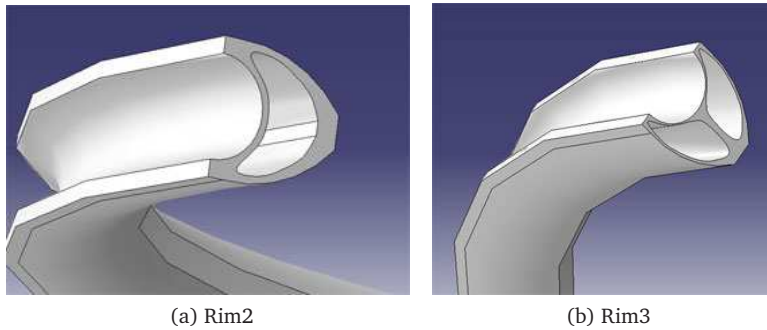


Figure 12: Explicitly Defined Rim Cross Sections

displayed). Figure 11 presents a time series of cutaway views at the pinched region of the rim. During the compression, there is a roughly constant reaction force of 60 kN from the deforming rim.

The second rim is created using 3D solid elements, and the cross-section is explicitly defined, as shown in Figure 12a . The maximum thickness is 1.65 cm and the minimum 0.5 cm. This rim has a calculated mass of 134 kg. Figure 13 presents a time series of cutaway views during compression. The reaction force from this rim is roughly constant at 200 kN.

The final rim also utilizes 3D solid elements, but the cross section is split into two cells, as shown in Figure 12b. The rim has a maximum thickness of 1.1 cm and a minimum thickness of 1.3 mm. This rim has a calculated mass of 88 kg. Figure 14 presents a series of cutaway views during compression. The reaction force of this rim is no longer constant, but varies from 120 kN at minimal compression to 150 kN at 1 m of compression, and then up to 400 kN at 1.5 m of compression. It also appears this rim design, under compression, distributes stress to the outside of the rim, eliminating the pressure points seen in the first two rims, which may lead to material failure in these regions.

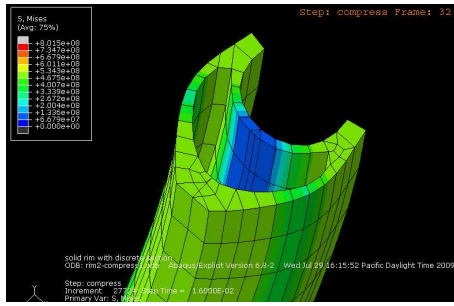
Given the mass of this rim, however, it would be reasonable to look into using a smaller wheel in the prototype light vehicle design, as well as investigate the possibility of utilizing aluminum rather than steel as the structural material.

### 3.7 Creating a Spoked Wheel with MAKESPOKES.PY

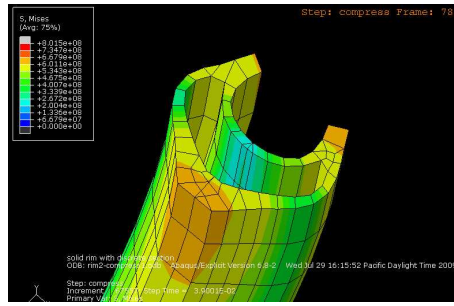
A method for modeling spokes has been validated and a candidate rim design identified. We now wish to put these parts together to form a spoked wheel model. The standard spoking pattern on bicycle wheels is known as the “3-cross” pattern. This pattern consists of 36 spokes angled to allow effective torque transfer from the hub to the rim without substantially sacrificing radial stiffness of the wheel[6].

In a bicycle wheel, spokes are also pre-tensioned such that when weight is placed on the hub, the bottom spokes retain some amount of tension, maintaining the shape of the wheel. Although it does not appear possible to define pre-tension via material definition in ABAQUS, it is possible to use a small actuating connector between one end of the spoke and its attachment point to explicitly create tension in the spoke at the

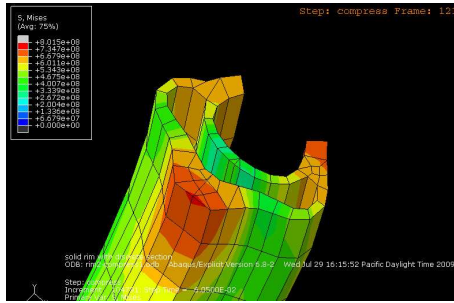




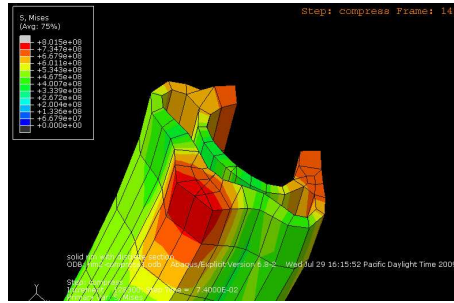
(a)  $t = 16$  ms



(b)  $t = 39$  ms

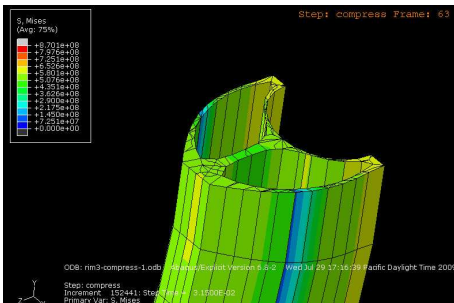


(c)  $t = 60.5$  ms

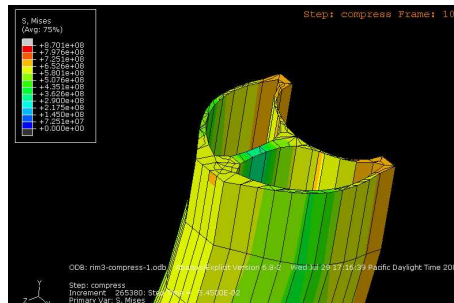


(d)  $t = 74$  ms

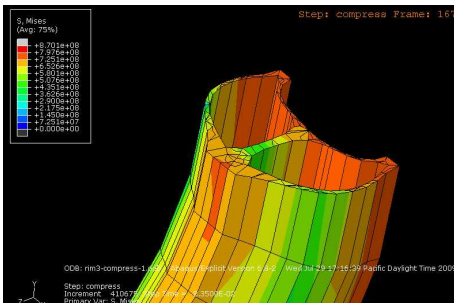
Figure 13: Rim2 Compression, Cutaway Views



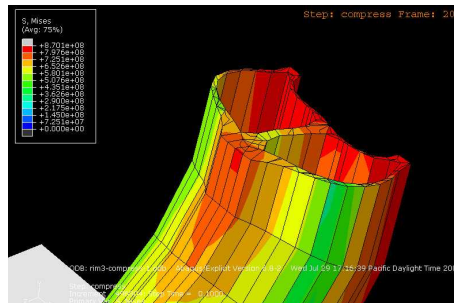
(a)  $t = 31.5$  ms



(b)  $t = 54.5$  ms



(c)  $t = 83.5$  ms



(d)  $t = 100$  ms

Figure 14: Rim3 Compression, Cutaway Views

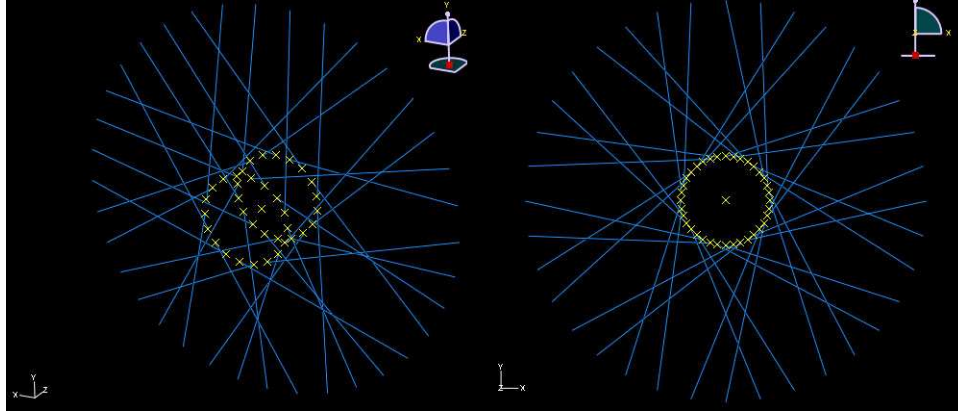


Figure 15: MAKESPOKES.PY Example Output

beginning of a simulation run. For the 2 m diameter rims used, actuating connectors with a length of a few millimeters are sufficient.

Conveniently, ABAQUS utilizes a PYTHON-based scripting language through which it is possible to automate such tasks as part creation and assembly. The PYTHON script MAKESPOKES.PY was created to programmatically generate a pattern of spokes within a specified ABAQUS model and then attach the actuating connectors needed to tension the spokes. Parameters definable for the script include number of spokes, actuator length, hub size and location, rim size, spoke dishing, and cross number. Thus, MAKESPOKES.PY can generate a variety of different spoke patterns. Example output of this script is presented in Figure 15 . The actuating connectors are too small to see in this figure.

### 3.8 Collision Testing of Spoked Wheel Designs

After generating a spoke pattern using MAKESPOKES.PY, the spokes are attached via spot-welds to a rim and hub to form a complete spoked wheel. A number of collision simulations were performed on these spoked wheels to investigate their behavior in collision with a car-hood shaped “collision profile”. Because a validated vehicle mesh had not been successfully imported into ABAQUS for this project, we substitute for a car hood two rigid plates joined at an angle, representing the frontal profile of the hood. Figure 16 illustrates the setup. The spoked wheel’s hub is a rigid body incorporating a point mass representing both the mass of a hub-motor and a fraction of the forward mass of the light vehicle.

The scenario we want to model consists of the wheel rolling towards the collision profile at a velocity of  $20 \frac{m}{s}$ , as measured at the hub. Defining initial conditions to actualize this initial velocity, however, was more complex than it at first seemed. The 1D truss elements used to define the spokes in the wheel do not support the use of angular velocity boundary (initial) conditions. It was impractical, however, to bring the wheel up to speed by applying a linear velocity to the center of the hub. If the acceleration applied is too great, the spokes would snap, and if it is too low, computational time would be wasted simulating acceleration of the wheel.

The solution was to create a datum cylindrical coordinate system centered at the bottom of the wheel such that the  $\theta$  axis of the coordinate system lay parallel to the axis of the wheel. Then each node and element in

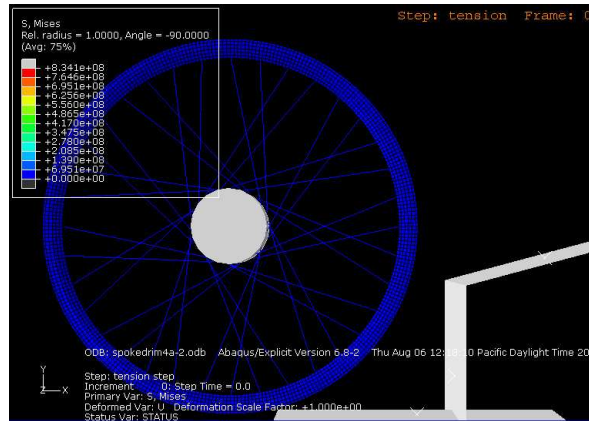


Figure 16: Spoked Wheel and Collision Profile Setup

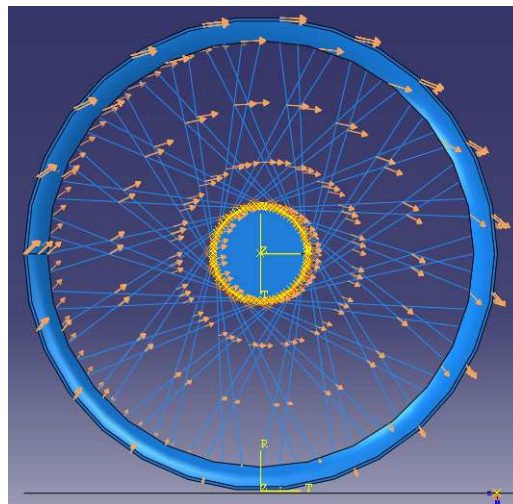
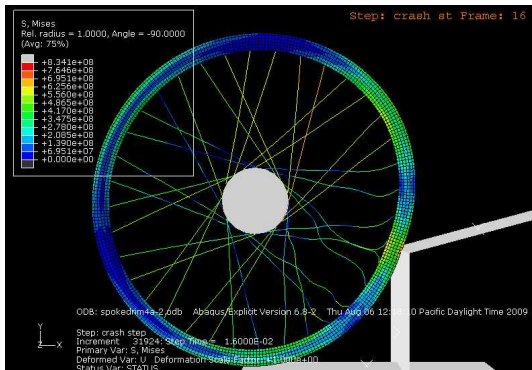


Figure 17: Illustration of Spoked Wheel Boundary Conditions

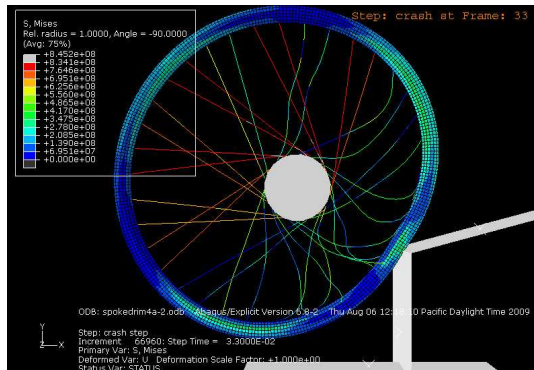
the wheel could be given an initial linear velocity in directions tangential to the datum coordinate system's radial direction, and with magnitudes proportional to the distance from the center of the datum coordinate system. A schematic representation of such a boundary condition is shown in Figure 17 .

In summary, the simulation initializes as follows:

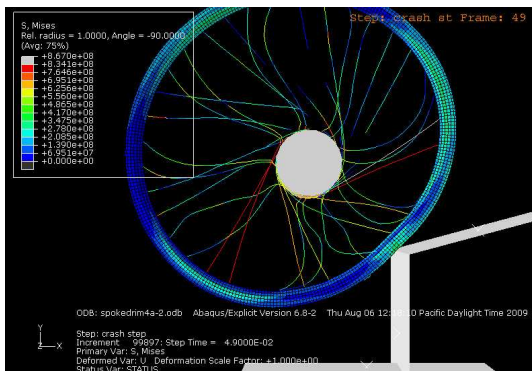
- In the interval of a few milliseconds, gravity is initialized in the system, allowing the wheel to fall and contact the ground. Gravity remains active for the subsequent duration of the simulation.
- During this same time interval, the actuating connectors pre-tension the spokes by 5 mm. These actuators remain in tension for the subsequent duration of the simulation.
- After pre-tension is completed, boundary conditions to give the wheel an initial velocity are applied during a one time-step (sub-millisecond) interval.
- The wheel is released from the boundary conditions and allowed to roll towards the collision profile.



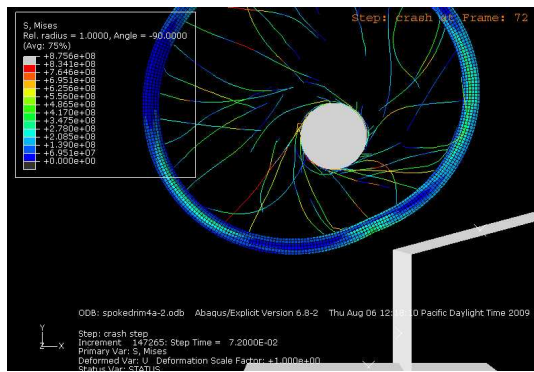
(a)  $t = 16$  ms



(b)  $t = 33$  ms



(c)  $t = 49$  ms



(d)  $t = 72$  ms

Figure 18: Spoked Wheel Collision Simulation,  $v_0 = 20 \frac{m}{s}$

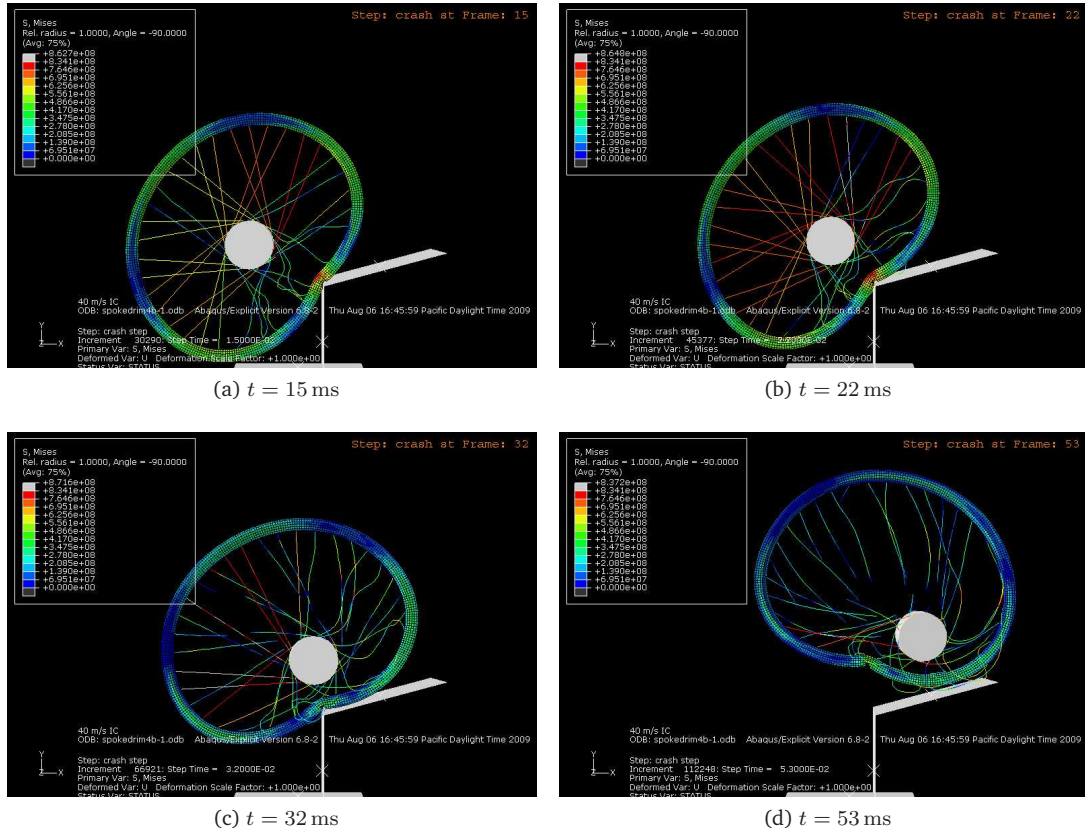


Figure 19: Spoked Wheel Collision Simulation,  $v_0 = 40 \frac{m}{s}$

Results from the first simulation at a number of time steps are presented in Figure 18 . Recall that the rim and spokes are defined with a DP590 material definition incorporating element failure, and that the rim has the split cross-section discussed earlier. As the wheel contacts the collision profile, the rim deforms and spokes to the rear of the hub begin to fail. As the wheel clears the top edge of the collision profile, the front spokes also fail as the hub and point mass continue to spin. It is uncertain whether these results are directly comparable to the collision behavior of the spoked wheel when it is connected to the front of a vehicle.

Additionally, the hub exhibits angular acceleration in the clockwise direction as spokes fail. It is possible that due to the angular momentum of the hub, spokes leaning counter-clockwise undergo plastic deformation earlier, and fail sooner than the clockwise leaning spokes. The clockwise spokes, then, accelerate the hub in a clockwise direction as their internal tension is released. This explanation is partially corroborated by a second simulation in which no pre-tension is defined in the spokes. In this scenario, the hub undergoes much less angular acceleration following failure of the spokes. It remains to be seen whether this phenomenon still persists when the extraneous mass is removed from the hub and the hub attached to the front of a light vehicle model instead.

Finally, a simulation was conducted in which the spoked wheel assembly is given an initial velocity of  $40 \frac{m}{s}$ . Results at a number of sequential time-steps are shown in Figure 19 . Upon collision, the spokes quickly fail, and the hub undergoes little significant deceleration. It is worth noting here that mesh elements of the rim in direct contact with the collision profile also fail. The collision profile is not representative of structural

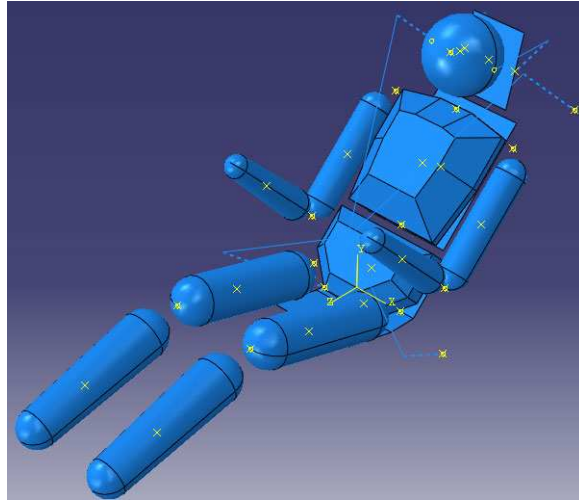


Figure 20: Crash Dummy Model Setup

characteristics of the front of an actual passenger sedan. Nonetheless, it may be sufficient for use in such scenarios where we are primarily interested in measuring the impact absorption characteristics of spokes in the wheel, rather than the rim.

### 3.9 A Simple Crash Dummy Model

The National Highway Traffic Safety Administration (NHTSA) has specific guidelines concerning the magnitude and duration of forces which an automobile passenger is subject to in frontal and side collisions[1, 2]. To evaluate the performance of a prototype light vehicle in context of these NHTSA requirements, a simple crash-dummy model has been developed to allow for measurement of forces on various parts of a passenger's body as a collision progresses. In the end, this crash-dummy model will be combined with a simple model of a two-wheeled vehicle frame, onto which the spoked wheels will be attached. The combined model will then be tested in a direct frontal collision with a car-hood profile target, and accelerations will be measured in the head, torso, and pelvis of the dummy.

The model consists of 11 rigid body parts connected by frictionless ball-and-socket joints, as shown in Figure 20 . The range of motion of the joints is not constrained – this should not have an appreciable effect on the forces experienced by the head, torso, and pelvis. Physical parameters for the body parts are summarized in Table 3 . It should be noted that these parameters are rough estimates. Lacking available anthropomorphic data, masses for body parts are estimated, and rotational moments of inertia calculated by approximating body parts as cylinders, rectangular blocks, and spheres.

A simulation is conducted to characterize the behavior of this dummy model while undergoing deceleration. The crash-dummy is positioned on a rigid seat and held in place by a four-point harness. In addition, the “head” of the dummy is harnessed to the headrest, representing a Head and Neck Support (HANS) device. This is similar to the HANS device used in F1 racing, in which a driver's helmet is secured to a collar behind the head by two straps. Both body and head harnesses are modeled with truss elements, which hold tensile stress but not bending or compression stress.

Part	Mass (kg)	$I_{zz}$ (kg · m <sup>2</sup> )	$I_{yy}$ (kg · m <sup>2</sup> )	$I_{xx}$ (kg · m <sup>2</sup> )
Head	4.5	0.018	0.018	0.018
Upper Arm	4.5	0.0036	0.0477	0.0447
Lower Arm	2.3	0.0015	0.0242	0.0242
Upper Torso	20	0.2082	0.3413	0.2082
Lower Torso	17.2	0.1613	0.1863	0.0896
Upper Leg	11.3	0.0203	0.2009	0.2009
Lower Leg	6.8	0.0107	0.1201	0.1201

For the crash dummy standing upright, local coordinates on each body part are defined such that  $z$  points vertically upward,  $y$  points forward, and  $x$  points to the left.

Table 3: Crash Dummy Model Parameters

The harness material is given a density of  $200 \frac{\text{kg}}{\text{m}^3}$ , a modulus of elasticity of 1 GPa, a Poisson ratio of 0.2, and a small amount of dampening to avoid transient force spikes when the harness is loaded during deceleration. This model uses globally defined hard-contact between all surfaces, with a static coefficient of friction of 1 and a dynamic coefficient of friction of 0.8. During the initialization process in simulation, the harness is tightened about the crash-dummy during a time-interval 100 ms. The pilot, seat, and harnesses are then given an initial velocity of  $20 \frac{\text{m}}{\text{s}}$ . Finally, the seat is smoothly decelerated from  $20 \frac{\text{m}}{\text{s}}$  to stop. Results from a number of sequential time steps are presented in Figure 21 .

Deceleration measurements taken at various nodes on the crash dummy, however, reveal transient spikes at almost every other time step. The amount of noise from these transients renders the deceleration data practically useless. It has been suggested in literature that, in finite-element simulations, measurement of force in a body undergoing accelerations is best conducted with a “virtual accelerometer” instead of measuring forces directly at elements or nodes[7]. In ABAQUS, it seems this can be accomplished by modeling a small rigid mass and attaching it via a spring connector (or another connector with suitably linear response) to the part in which force is to be measured. Monitoring the length of this connector will yield indirect measurements for force, which hopefully lack the transient spikes seen in direct force measurements. Unfortunately due to time constraints, work in this direction was not completed.

### 3.10 Creating the Light Vehicle Prototype

A representation of the light vehicle model prototype was constructed towards the end of this study, as shown in Figure 22 . The rims in this final model are represented using 2D shell mesh elements for computational efficiency. This model was intended to test variation in crash behavior as a function of wheel diameter. It was also intended to yield first-approximations of forces experienced by the occupant in the event of vehicular collision. Due to time constraints, however, this portion of the project was left incomplete.



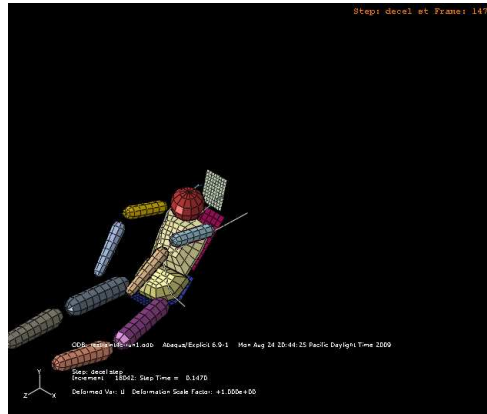
(a)  $t = 46$  ms



(b)  $t = 148$  ms

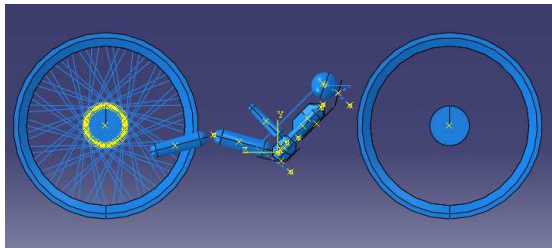


(c)  $t = 182$  ms

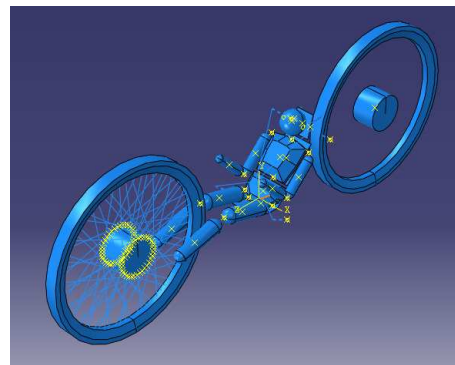


(d)  $t = 247$  ms (almost stopped)

Figure 21: Crash Dummy Model Deceleration Simulation



(a) Side View



(b) Perspective View

Figure 22: Light Vehicle Model Schematic



## **4 Recommendations for Future Work**

Future work on this model would entail conducting simulations of the prototype light vehicle model developed. A rigid-body constraint would be used to join the hub axes and seat, representing an ideal rigid frame, to a point mass representing the remaining mass of the vehicle. The entire assembly would then be tested in collision against the previously discussed collision profile. Measurements for deceleration pulse on various parts of the crash-dummy would be compiled in order to determine the maximum velocity for which the vehicle is able to protect the occupant at NHTSA standards. From there, a number of different directions may be pursued to better characterize crash behavior of the model, or to optimize occupant protection characteristics.

### **Impact of Steering Mechanism on Collision Characteristics**

The bare-bones vehicle model developed does not include any representation of a steering device. A steering mechanism is eminently necessary for a viable vehicle design, and to balance a two-wheeled vehicle in motion, this steering mechanism must also prove dynamically stable. There are a number of different options for implementing a stable steering mechanism for this type of vehicle. Each would have implications for the collision behavior, and consequently the occupant protection capabilities of the vehicle.

A number of steering implementations would need to be investigated. A few promising candidates should be chosen and incorporated into the vehicle model to investigate the changed collision behavior. It may become necessary to incorporate a steering-locking mechanism which engages upon vehicular impact to lend more rigidity to the light vehicle frame.

### **Modeling a Protective Occupant Cage**

The model as developed thus far does not include a protective cage for the occupant. Such a cage is absolutely necessary for occupant protection in a road vehicle, and must be designed to be as rigid and crush resistant as possible. Although it does not seem that an occupant cage would significantly change collision behavior of the vehicle, there are a number of space and mass constraints imposed by the layout of the vehicle design which need to be taken into consideration.

Simulation of the vehicle with the occupant cage should examine the behavior of the vehicle after initial collision. There is a good possibility that a secondary collision will occur in which the occupant cage impacts the colliding vehicle. The cage must be designed to undergo minimal deformation during such an impact.

### **Designing a Seat Lifting Mechanism for Occupant Protection**

A mechanism for swinging or lifting the occupant of a light vehicle over the impact and crush zone during a collision may prove the key to occupant protection in a head-on collision with a heavy vehicle. Such a

mechanism must be capable of lifting both the occupant and the protective cage in which the occupant sits within tens of milliseconds. There are a number of directions one may pursue towards this end.

The occupant cage may be mounted on a hinge system, designed such that frontal impact with the light vehicle would cause the cage to swing upward. An explosive charge may alternatively be used to propel the cage and occupant upward. It is possibly relevant in this scenario to investigate biomechanical response in ejection-seat passengers. Finally, the rear end of the light vehicle may be designed hinged in such a way as to allow the rear end to rotate upward in a frontal collision, lifting the occupant cage along with it.

## 5 Environmental Applicability and Concluding Remarks

Although modern electric vehicles such as the Chevrolet Volt and the Nissan Leaf represent steps towards ostensibly cleaner and more efficient road vehicles, they also leave a good deal to be desired. Electric vehicles are not truly emissions-free - carbon dioxide not emitted by electric vehicles are generated instead at power plants in supplying the additional load needed to charge each electric vehicle. In addition, it is currently beyond the capabilities of our electricity generating infrastructure to support large-scale adoption of heavy electric vehicles. A more comprehensive approach towards emissions reductions and energy efficiency in the transportation sector entails adoption of not heavy electric vehicles, but *light* electric vehicles.

The United States Bureau of Transportation Statistics (BTS) reported in 2003 that the mean occupancy for all personal vehicle trips is 1.63. The seating availability in the average passenger sedan, electric or gas-powered, on the other hand, is 5. This extra seating represents unnecessary structural mass carried by the vehicle, translating in the end to wasted energy and unnecessary carbon emissions. It would be more prudent for a commuting public to utilize a mix of one- and two-seat vehicles, and to operate high-occupancy vehicles only when necessary.

The same BTS report points out that the average distance traveled daily by persons aged 15 and older is 29.1 mi. The driving range, however, for electric vehicles such as the Nissan Leaf is approximately 100 mi, and for high-end electric vehicles such as the Dodge Circuit EV and Tesla Roadster, approaches 200 mi. Excess driving range represents extra battery mass carried by the vehicle, resulting again in wasted energy and unnecessary carbon emissions.

The current archetype for respectable a road vehicle, which includes 5-person occupancy and 200 + mi range, is a standard inherited from our legacy of gasoline-powered automobiles. Transitioning on a large scale to electric vehicles which fit this archetype does not constitute a leap forward in human-transportation technology, but merely a step to the side. Real progress would consist today of developing electric vehicles best described as "1/3-cars", seating one or two people and capable of driving 50 – 100 mi on a single charge. The prototype light vehicle design investigated in this study represents a possible direction towards realization of such a 1/3-car.

The key factor, however, governing the ultimate viability of such light vehicles as replacements for gasoline-powered automobiles, is the degree of protection they afford occupants in collision against heavier vehicles. The author would like to emphasize that safety should serve as a foundation stone in the design of such light vehicles.

## 6 Acknowledgments

The author would like to express sincere gratitude to Professor Mary Cardenas of Harvey Mudd College for sponsoring this project, providing technical guidance, and offering emotional support. Furthermore, the author would like to thank Professor Joe King of Harvey Mudd College for invaluable advice in the conception and design of the prototype vehicle discussed in this work. The author would also like to acknowledge Jack Knipe of Southern California Edison's Electric Vehicle Technical Center for assistance in investigating mass distribution in electric vehicles.

Finally, the author is grateful for the support provided by the Center for Environmental Studies at Harvey Mudd College. This study was made possible by a research grant provided by the Center for Environmental Studies in the summer of 2009.

## 7 Appendix: Accessing the Online Research Journal

An online blog-style journal was used during the course of this project to record progress in a manner easily accessible by others. This journal includes

- ABAQUS source files
- Animations of key results from each portion of this study
- A select number of literature reviews on background readings
- General project notes
- Links to reference documents and sites
- Downloadable versions of the PYTHON scripts developed for this project

The journal, as well as all incorporated files, figures, and animations, are secured against public viewing by password. Once logged in, however, the user is given access to all of these until the browser is closed. The research journal may be accessed with the following:

<b>URL</b>	<code>http://stevenning.com/ces2009/</code>
<b>User</b>	<code>viewer</code>
<b>Password</b>	<code>hmc6238</code>

## References

- [1] National Highway Traffic Safety Administration. 571.208 standard no.208; occupant crash protection. In *Federal Motor Vehicle Safety Standards and Regulations*. US Department of Transportation, 2004.
- [2] National Highway Traffic Safety Administration. 571.214 standard no.214; side impact protection. In *Federal Motor Vehicle Safety Standards and Regulations*. US Department of Transportation, 2004.
- [3] Jorge Ambrosio. Contact and impact models for vehicle crashworthiness simulation. *International Journal of Crashworthiness*, 8:73–86, 2003.
- [4] autocar.co.uk. Chevrolet volt in final phase. Online News Article, August 2008. <http://www.autocar.co.uk/News/NewsArticle/Chevrolet-Concepts/234534/>.
- [5] Michael Berenis. Nissan leaf performance modifications. Online Article, August 2009. <http://www.examiner.com/examiner/x-4824-Tampa-Sports-Car-Examiner-y2009m8d2-Tuning-review-Nissan-LEAF>.
- [6] Jobst Brandt. *The Bicycle Wheel*. Avocet, 1995.
- [7] Z. Q. Cheng, J. G. Thacker, W. D. Pilkey, W. T. Hollowell, S. W. Reagan, and E. M. Sieveka. Experiences in reverse-engineering of a finite element automobile crash model. *Finite Elements in Analysis and Design*, 37:843–860, 2001.
- [8] H. Hooputra, H. Gese, H. Dell, and H. Werner. A comprehensive failure model for crashworthiness simulation of aluminum extrusions. *International Journal of Crashworthiness*, 9:449–464, 2004.
- [9] H. S. Kim and H. Huh. Vehicle structural collapse analysis using a finite element limit method. *International Journal of Vehicle Design*, 21:436–449, 1999.
- [10] Art Michalik. Nissan leaf versus gm ev1: how much have electric cars improved in 10 years? Online News Article, August 2009. <http://www.examiner.com/x-11005-San-Jose-Sports-Car-Examiner-y2009m8d2-Nissan-LEAF-versus-GM-EV1-what-a-difference-10-years-makes>.
- [11] K. Vedantam, D. Bajaj, N. S. Brar, and S. Hill. Johnson-cook strength models for mild and dp 590 steels. *Shock Compression of Condensed Matter*, pages 775–778, 2005.